The Effect of Varying Enclosed Area and Age-Adjusted Cortical Bone Properties on the Structural Response of the Rib: A Simulation Study

Kevin M. Fleischmann, Fang-Chi Hsu, Jazmine R. Aira, F. Scott Gayzik

Abstract Recent studies have explored error introduced through rib segmentation, which suggest possible overestimation in cross-sectional area of human rib computational models due to the resolution of full-body CT scans. Additionally, there is a need to explore age effects on rib response through simulation. In this study, we observe the effects of varying enclosed area, age-related properties, and shell thickness scheme through simulation to gauge the effectiveness of methods of translating geometry and measured material properties of bone to computational models.

A computational model of the right 6th rib was isolated and adjusted for 128 test models (8 area adjustments x 8 cortical materials x 2 shell thickness projections). Regression equations for age-related cortical properties were taken from recent literature. The cortical surface was projected inward from the baseline model to reduce enclosed area. A constant velocity of 0.5 mm/ms was applied at the anterior end. The posterior end was pinned.

Six dependent variables were measured. Differences were observed between groups in all independent variables. Age effects and area reduction were significant in stiffness, displacement at fracture, peak force, force at yield, and energy absorbed. Area reduction was also significant in displacement at yield. The highest R^2 was found in the linear model for stiffness. The study suggests that overestimation of the enclosed area and accounting for age through age-related properties will affect the mechanical response of rib models.

Keywords Aging, cortical bone mapping, rib, simulation, thoracic impact.

I. INTRODUCTION

One of the most common phenomena in motor vehicle crash (MVC) scenarios is high-rate mechanical loading of the thorax. Preventative measures for thoracic injuries in modern vehicles include safety systems that interface with the chest and ribs. Nonetheless, rib fractures are one of the most common injuries experienced in such scenarios [1]. These injuries have high rates of morbidity and mortality, especially in older populations [2][3]. Additionally, studies have shown that these injuries can be predicted using a variety of factors among which is geometry [4-7]. Thus, there is an increasing need to understand the biomechanics of thoracic tissue across age groups as well as to capture the morphology of the structure as accurately as possible. When exploring rib fracture and thoracic injury through simulation, the ribs must be modelled both geometrically and material-wise with the best available data in order to ensure accurate information on the associated injury mechanism [6].

Computed tomography (CT) is one method of obtaining information regarding the geometry of the thoracic region. With regard to the ribs, CT imaging can be used to obtain cortical bone shape data. This step is important, as rib fracture is defined by the response of the cortical bone, which is dependent not only on material properties but also on geometry. Full-body CT images are used in a number of ways to establish a geometry of the rib. A few of these methods are segmentation partially automated through thresholding and as inputs to cortical bone mapping (CBM) algorithms, which provide a blueprint that is used to establish realistic computational models.

Some of these methods, however, can have a rather high variability, as pixel sizes in typical full-body CT scans are relatively large when visualising small structures such as the ribs. When comparing CBM with full-body CT segmentation partially automated through thresholding techniques in particular, full-body CT segmentation seems to have higher associated errors. Recent work has studied the differences in these techniques and has shown higher accuracy of CBM [8]. In other recent studies, uncertainty of rib geometry measurement has been

Kevin M. Fleischmann (+1 412 327-4814, kfleisch@wakehealth.edu) is a PhD student in Biomechanical Engineering, Fang-Chi Hsu is a Professor of Biostatistics and Data Science, Jazmine R. Aira is a Research Engineer in Biomedical Engineering, and F. Scott Gayzik is an Associate Professor of Biomedical Engineering at Wake Forest University School of Medicine in Winston-Salem, NC, USA.

explored [9]. The referenced study seeks to quantify error associated with full-body CT scans – and that work has proposed an average overestimation in rib cross-sectional area (CSA) in human body models of up to 39%.

The Global Human Body Models Consortium (GHBMC) family of full human body computational models has been in development for over ten years. The rib geometry utilised in these models was obtained using partially automated segmentation techniques from full-body CT images. The GHBMC M50-O is the baseline model used in this work, representing the body geometry of a 50th percentile male, and for which bone geometry has been constructed from full-body CT of a 26-YO person and an appropriate cortical thickness applied per the literature [10-12]. Given the methods used to generate this model, which are typical for full human body models (HBMs), there is a need to study the effects of possible error or overestimation in the total CSA (Tt.Ar) of the rib geometry. It is important to note that this aspect of the study is not related to the aging process, but rather explores the effect of potential overestimation of the baseline geometry itself.

However, in many recent studies, changes in rib morphology and structural properties with age and their effects on thoracic injury have been studied [13][14]. Since the behaviour of rib models is a function of geometry, mesh and material properties, it is also important to consider changes in rib cortical bone elastic-plastic constitutive properties with age and shell area. Reference [15] has correlated the effects of aging to the elastic-plastic constitutive properties of the rib cortical bone. In that study, rib post-mortem human subject (PMHS) samples from subjects across ages underwent material testing and regression equations of property versus age were fit to the properties of elastic modulus, ultimate stress, and failure strain, among others. The material properties of the rib cortical bone of the GHBMC M50-O are the result of an optimisation study, reference [16], to match Young's modulus, yield stress, tangent modulus, and failure strain of the model to the force-displacement curve in experimental loading of the 4th rib to minimise mean square error. These properties have been calibrated to no particular age [17]. Due to the additional effects of age on prevalence of thoracic injury in MVCs, there is a need to further explore the effects of altering these properties.

Thorax injuries are common in MVCs, and the study of rib fractures and other thoracic injuries is a prime application for human body models, but the effects of cortical mapping uncertainty on simulation response have yet to be explored. This simulation-based study attempts to quantify rib biomechanical response as a function of enclosed area, second moment of area of the cortex, and constitutive properties of cortical bone. These results will help determine the extent to which the ribs of full human body models are affected by potential anatomical bias introduced by the use of whole body CT while also factoring in material and numerical considerations.

II. METHODS

The model adjustment and simulation setup methods were developed internally. The right 6th rib was extracted from a full HBM computational model (GHBMC M50-O v5.0) using LS-PrePost v 4.6.7 (LSTC, Livermore, CA, USA). Two individual parts were extracted and included in the extracted test model: a two-dimensional (2D) shell part representing the cortical bone of the rib and an enclosed three-dimensional (3D) solid part representing the cancellous bone. A matrix of 128 simulations varying three parameters (8 Tt.Ar adjustments × 8 cortical materials × 2 shell thickness methods) was developed. This is shown in Table I below.

TABLE I

TEST MATRIX. ONE SIMULATION PER TABLE ENTRY WAS RUN. THE *B* COLUMN IS FOR THE BASELINE GHBMC MODEL, REPRESENTING NO SPECIFIC AGE. THE COLUMNS *20*, *30*, …, *80* REFER TO AGE-RELATED MATERIAL PROPERTIES AT THE STATED AGE.

		nloc 1									*nloc* 0								
		Age									Age								
		B	20	30	40	50	60	70	80		B	20	30	40	50	60	70	80
CSA Reduction	*0 mm*	x	x	x	x	x	x	x	x	*CSA Reduction*	*0 mm*	x	x	x	x	x	x	x	x
	0.2 mm	x	x	x	x	x	x	x	x		*0.2 mm*	x	x	x	x	x	x	x	x
	0.4 mm	x	x	x	x	x	x	x	x		*0.4 mm*	x	x	x	x	x	x	x	x
	0.6 mm	x	x	x	x	x	x	x	x		*0.6 mm*	x	x	x	x	x	x	x	x
	0.8 mm	x	x	x	x	x	x	x	x		*0.8 mm*	x	x	x	x	x	x	x	x
	1.0 mm	x	x	x	x	x	x	x	x		*1.0 mm*	x	x	x	x	x	x	x	x
	1.2 mm	x	x	x	x	x	x	x	x		*1.2 mm*	x	x	x	x	x	x	x	x
	1.4 mm	x	x	x	x	x	x	x	x		*1.4 mm*	x	x	x	x	x	x	x	x

Methods of loading were adapted from a PMHS experimental rib loading study [18]. Each rib model was oriented for loading in a 2D plane; that is, the pitch angle of the ribs relative to the anatomical transverse plane was accounted for by positioning anterior and posterior ends in the same XY-plane and loading along the X-axis only. The posterior end of the rib was constrained such that it can rotate in the XY-plane but not translate, mimicking a pin joint. A bending load was applied by adding a constant velocity of 0.5 mm/ms along the loading axis to a node set at the anterior end of the rib.

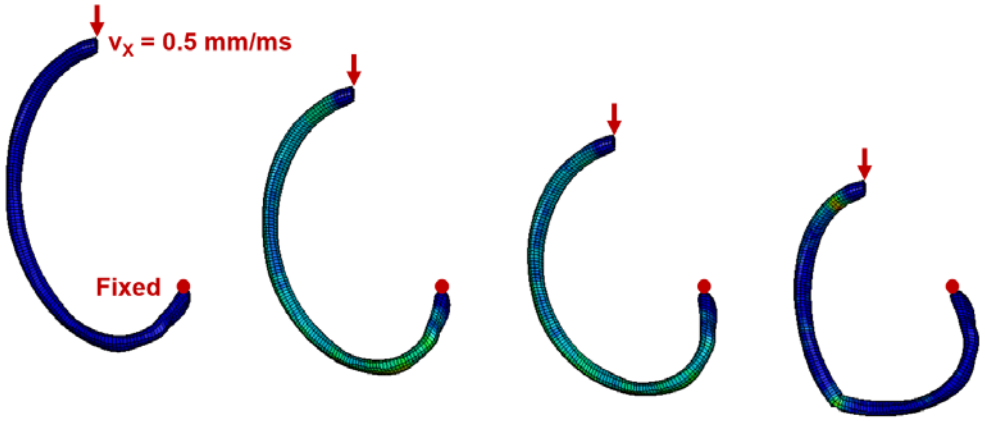

Fig. 1. Loading method for all 128 simulations.

Adjustments were made to the models as follows. For age adjustments, regression equations from [15] were utilised. Equations estimating Young's modulus, yield stress, and failure strain of rib cortical bone were adapted from the paper, with ages ranging from 20 to 80 years entered as inputs in steps of a decade. Tangent modulus was also adapted according to regression equations in [15]. The failure stress, failure strain, yield stress, and yield strain for each age point was calculated from the individual regression equations of those parameters, and the slope (i.e. the change in stress over the change in strain) between the yield point and failure point was taken as the tangent modulus for that age. One baseline model and seven age-adjusted models (20, 30, 40, 50, 60, 70, 80 years) were produced in order to compare the response of the model among eight groups of age-based cortical bone material properties. All models used a piecewise linear elastic model with failure. Failure of models occurred when the failure threshold for strain was reached. For the baseline GHBMC model, this strain was 18000µ per [16], and for the models age-related material properties, these strains were calculated per the regression equations in [15], ranging from 19568µ to 39923µ.

Models with reduced enclosed CSA of the rib were created to test for effects of possible overestimation. The reduced-Tt.Ar 6th rib computational models were created by applying an inward projection of the node set of the 2D cortical shell elements of the baseline rib model. The inward-facing normal direction of each quadrilateral shell element was calculated, and the corresponding nodes were projected in that direction by a fixed amount. The amount of inward projection ranged from 0.0 mm to 1.4 mm in steps of 0.2 mm. An adjusted node set was saved and defined as a boundary-prescribed final geometry. Simulations were then run using LS Dyna v 10.0 (LSTC, Livermore, CA, USA) to shrink the entire rib model to this geometry, which ensured that the inner nodes of the solid elements were shrunk proportionately to the outer shell elements.

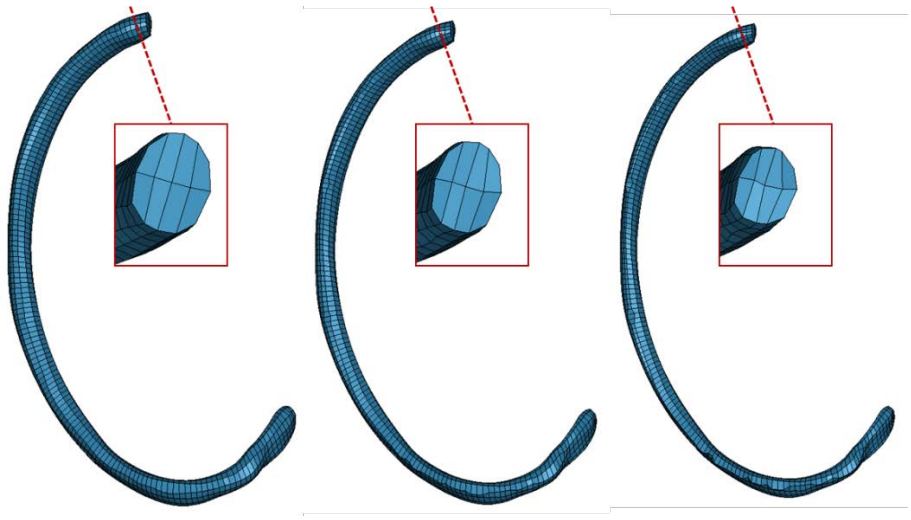

Fig. 2. Graphic of baseline vs. reduced-Tt.Ar models (two of seven shown) of whole rib with cut section callouts. From left to right: baseline model with no CSA reduction, 0.8 mm of inward projection for CSA reduction, and 1.4 mm of inward projection for CSA reduction.

The number of 0.2 mm inward projection steps necessary to obtain a given reduction in Tt.Ar was determined by measuring the overall CSA reduction at each CSA reduction step. Based on data in [9] the overestimation in rib CSA based on measurements from full-body CT scans can be as high as 39%. Reduction in CSA of 39% as measured at three cross-sections of the rib occurred after 1.4 mm of inward projection. To test this as a representative reduction across a greater number of cross-sections of the rib, a more robust measure was taken at this level of inward projection by measuring the percentage change at 15 different cross sections, which were taken every ten elements (edge length approximately 2.3 mm per element). A reduction of 40% was measured using this method, so this geometry was deemed a sufficient representation of the reversal of the amount of the total potential overestimation. Additionally, average overestimation was found to be approximately 0.8 mm of inward projection [9] (24% difference in cross-sectional area for the GHBMC M50-O 6th rib), which was covered in our analysis as the midpoint of the steps of inward projection.

Shell element thickness was projected in two different ways for two placements of shell element thickness so that effects of second moment of area on the mechanical response could also be observed. Shell element thickness profile, however, remained unchanged. The profile used for all models in this study was developed from a dataset in [11] and accounts for variability in thickness across the surface of the rib (both across the length and within a cross section). Possibilities for alteration of shell element thickness were considered but omitted from the scope of this study, which is further discussed in the Discussion. The rib models in the GHBMC M50-O use inward projection from the 2D shell part for the cortical bone to be consistent with the segmentation methodology. Due to the effect of projection direction on the second moment of area, an altered form was developed in which the shell element thickness was projected equally about the shell surface. This was controlled in the model keyword file by updating the *nloc* variable. An *nloc* value of 1, as is in the original model, represents projection of shell element thickness inward, and an *nloc* value of 0 dictates equally projected shell thickness (Figure 3).

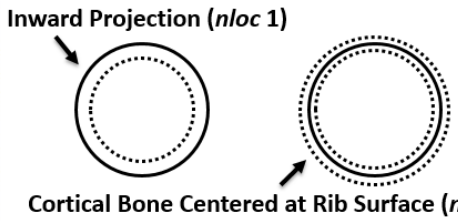

Fig. 3. Diagram that presents direction of shell element thickness projection when viewing a cross section of the rib. The solid line represents the boundary of the 3D solid part, and the dotted lines represent the boundary to which the shell element thickness is projected.

Simulations were run in LS Dyna v 10.0 (LSTC, Livermore, CA, USA). Simulations for all test cases were run until rib fracture. Following test runs, resultant force data over time was extracted from a single fixed node at the

posterior end of the rib. A 60 Hz SAE filter was applied to the data in LS-PrePost.

Extracting force versus time data allowed all dependent variables of interest to be studied after some analysis and calculation. The variables of interest were peak force, force at yield, stiffness, displacement at yield, displacement at fracture, and energy absorbed through loading. Methods of calculation of each variable were developed for this study. Fracture time was noted from the point at which force dropped slightly, after which bounce back due to restraint caused a spike in resultant force. Peak force was taken as the maximum force measured prior to fracture. Stiffness was calculated as the slope of the force-displacement curve between 0 and 20 ms, reliably within the elastic region of each test run. A material yield point was denoted where the force-displacement response began to change from elastic to plastic. As a repeatable method of determining this yield point, a line was calculated from the point of 90% of maximum force to the point of maximum force (plastic region). The intersection of this line with the stiffness line – with an offset applied to mimic calculation of a yield point on a stress-strain curve – was taken as the yield point.

For statistical analysis, three independent variables, i.e., age-related material properties, CSA reduction, and direction of shell element thickness, and six dependent variables, i.e., displacement at fracture, peak force, stiffness, displacement at yield, force at yield, and energy absorbed, were included in the analysis. To satisfy the normality assumption for regression modelling, the distributions of dependent variables were examined. The dependent variables were all normally distributed, so transformation was not needed. Linear regression models were used to determine the associations between the independent variables and dependent variables. All of the continuous variables, including age, CSA reduction, and six dependent variables, were standardised, i.e., minus mean and divided by standard deviation, for the purpose of relative importance. The standardised variables were rescaled to have a mean of zero and a standard deviation of one. Thus, the standardised regression coefficients could be compared across models and within models (only for continuous independent variables) qualitatively.

In order to identify which independent variables were most strongly associated with each dependent variable, stepwise selection was used to generate the final model including all the statistically significant independent variables. The most associated independent variable would be selected first. The p-value was to be less than 0.05 to be kept in the final model. The R^2 value that measured the proportion of variance of the dependent variable that is explained by the first selected independent variable was calculated. The partial R^2 value, which measures the proportion of the variance of the residuals of the dependent variable that is explained by the second selected independent variable, was also calculated. In other words, the partial R^2 value calculates the additional proportion of the variance that can be explained by the second independent variable given the first independent variable is fitted in the model. The same approach could be applied to calculate the partial R^2 for the third independent variable given the first two independent variables are fitted in the model. If the additional independent variable was not significantly associated with the dependent variable, its partial R^2 was not calculated. The overall R^2 for the final model was estimated as well. In summary, standardised regression coefficients, p-values, and partial R^2 were used to determine the most statistically significant independent variables for each dependent variable.

III. RESULTS

All 128 simulations normal terminated. A sample of four of the 128 results is shown in Figure 4, exhibiting a typical piecewise linear behaviour. In this example, results for a 20 year old, 40 year old, and 80 year old are plotted with inward shell area (*nloc* 1) and an inward diameter reduction of 0.8 mm. The baseline GHBMC 6th rib response is also plotted. The full mechanical results of the simulation matrix are provided in Table A I of the Appendix.

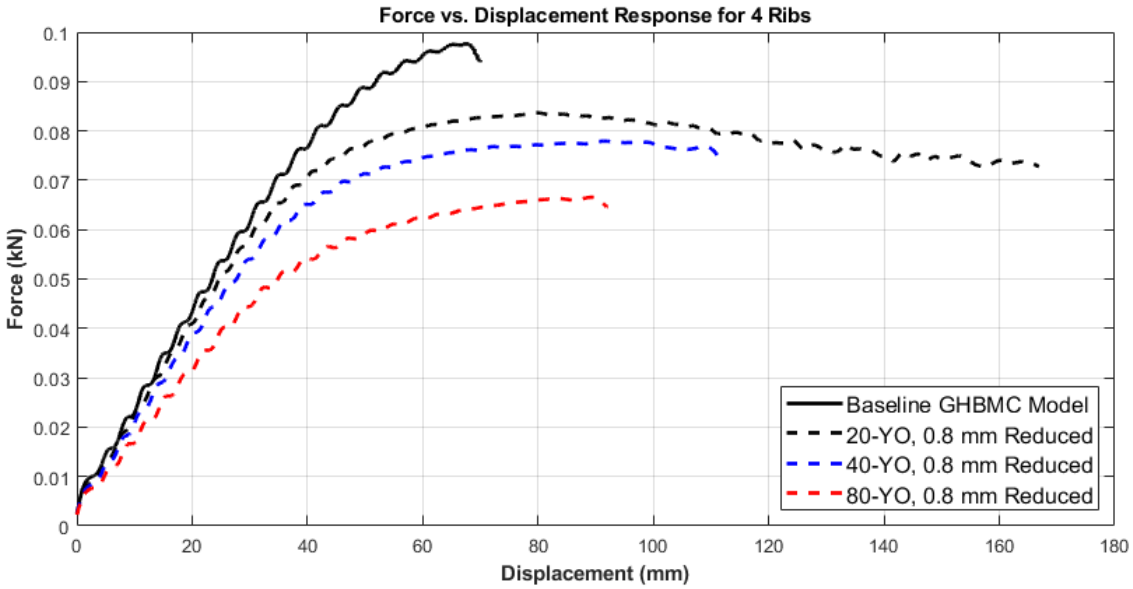

Fig. 4. Force response from onset of applied linear velocity until fracture in four of 128 test cases. Higher peak force was sustained by the baseline GHBMC model than 0.8 mm reduced models, slopes are similar for 20 and 40 year olds, but fracture occurred at a lower displacement. Stiffness response is fairly consistent with younger and middle-aged models.

The statistical analysis for all six dependent variables showed some level of significance of the independent variables for all dependent variables. The baseline model was not included in the statistical analysis as it was not designed for a specific age. This provided six different regression equations, each of which was explained by two or three of the independent variables. For displacement at fracture, the R^2 value when accounting for all independent variables was 0.85, and 69% of variance could be explained by the age term of the model ($p < 0.0001$). For peak force, the R^2 value was 0.98, and 72% of variance could be explained by the CSA reduction term ($p < 0.0001$). For stiffness, the R^2 value was 0.98, and 75% of variance could be explained by the CSA reduction term ($p < 0.0001$). For displacement at yield, the R^2 value was 0.86, and 73% of variance could be explained by the CSA reduction term ($p < 0.0001$). For force at yield, the R^2 value was 0.97, and 67% of variance could be explained by the CSA reduction term ($p < 0.0001$). For energy absorbed, the R^2 value was 0.83, and 69% of variance could be explained by the age term ($p < 0.0001$). The statistical analysis is summarised in Table II. Cumulative R^2 values for each regression model are in the bottom row. Recall the analysis was conducted on standardised values for comparative purposes of the various parameters.

TABLE II

STATISTICAL SUMMARY OF REGRESSION TESTS FROM ALL TEST RUNS. ALL P-VALUES ARE PRESENTED, AND SIGNIFICANT VARIABLES ARE PRESENTED WITH PARTIAL R^2 VALUES FOR THE CORRESPONDING REGRESSION MODEL. SHADED BOXES REPRESENT THE GREATEST PARTIAL R^2.

	Displacement at Fracture	Peak Force	Stiffness	Displacement at Yield	Force at Yield	Energy Absorbed
Age-Related Material Properties	$p < 0.0001$ $R^2 = 0.69$	$p < 0.0001$ $R^2 = 0.11$	$p < 0.0001$ $R^2 = 0.084$	$p = 0.1515$	$p < 0.0001$ $R^2 = 0.13$	$p < 0.0001$ $r^2 = 0.69$
CSA Reduction Projection	$p < 0.0001$ $R^2 = 0.15$	$p < 0.0001$ $R^2 = 0.72$	$p < 0.0001$ $R^2 = 0.75$	$p < 0.0001$ $R^2 = 0.73$	$p < 0.0001$ $R^2 = 0.67$	$p < 0.0001$ $R^2 = 0.035$
Shell Thickness Projection	$p = 0.0148$ $R^2 = 0.009$	$p < 0.0001$ $R^2 = 0.15$	$p < 0.0001$ $R^2 = 0.15$	$p < 0.0001$ $R^2 = 0.13$	$p < 0.0001$ $R^2 = 0.17$	$p < 0.0001$ $R^2 = 0.11$
Cumulative Correlation for Regression Model	$R^2 = 0.85$	$R^2 = 0.98$	$R^2 = 0.98$	$R^2 = 0.86$	$R^2 = 0.97$	$R^2 = 0.83$

As the statistics were obtained from a multiple linear regression model, it is somewhat difficult to see numerical effects of the association between variables through the individual R^2 values. For example, the relationship between stiffness and age-related material properties has an R^2 value of 0.084, which is the same whether a simple linear regression or a multiple linear regression is run (for multiple linear regression, this is the partial R^2 value). However, p-values presented are denoting significance within the multiple linear regression model, meaning that the correlation is clear enough that the given independent variable factors into the model response.

The visual effects of the independent variables are noticeable in graphical form. Plots for linear stiffness data are included below because stiffness had the largest R^2 value among tested variables, but similar trends are found in others. Figure 5 shows measured stiffness vs. CSA reduction with age within each group for all 128 simulations. Figure 6 shows measured stiffness vs. age with Tt.Ar adjustment within each group. The slope of the trend is greatest with adjustment of Tt.Ar, and at high levels of Tt.Ar adjustment age is less of a factor. In Figure 6, the GHBMC baseline model stiffness is also shown. Data for evenly projected shell element thickness followed similar trends but were left out of plots for simplicity to display graphs in two dimensions. The full results table is provided in the Appendix in Table AI. Graphs are plotted in tabular format in Tables AII and AIII.

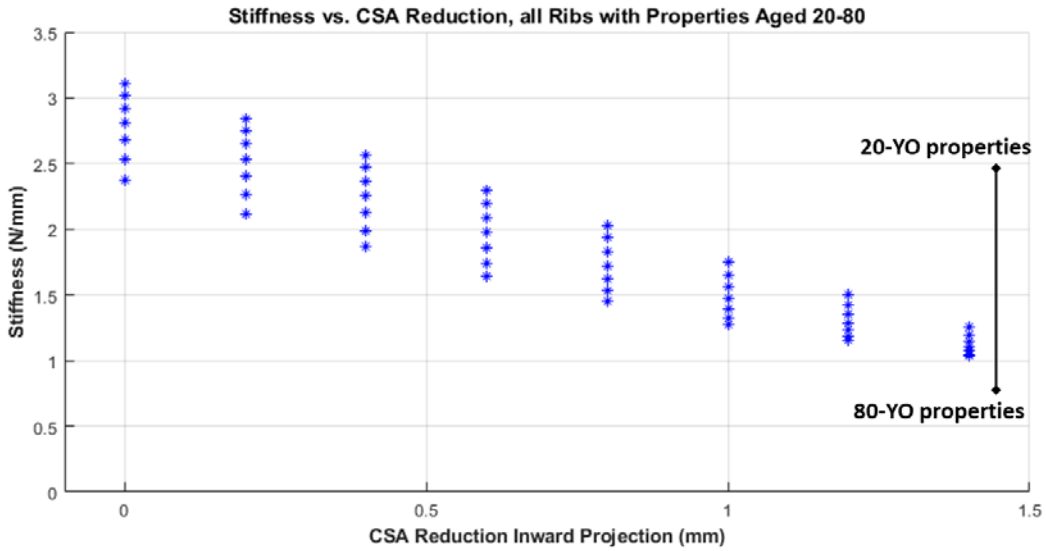

Fig. 5. Plotted data for stiffness vs. CSA reduction for all *nloc* 1 test runs. Highest data point in each Tt.Ar set represents the 20-YO model and lowest data point represents the 80-YO model, with each age lying in between.

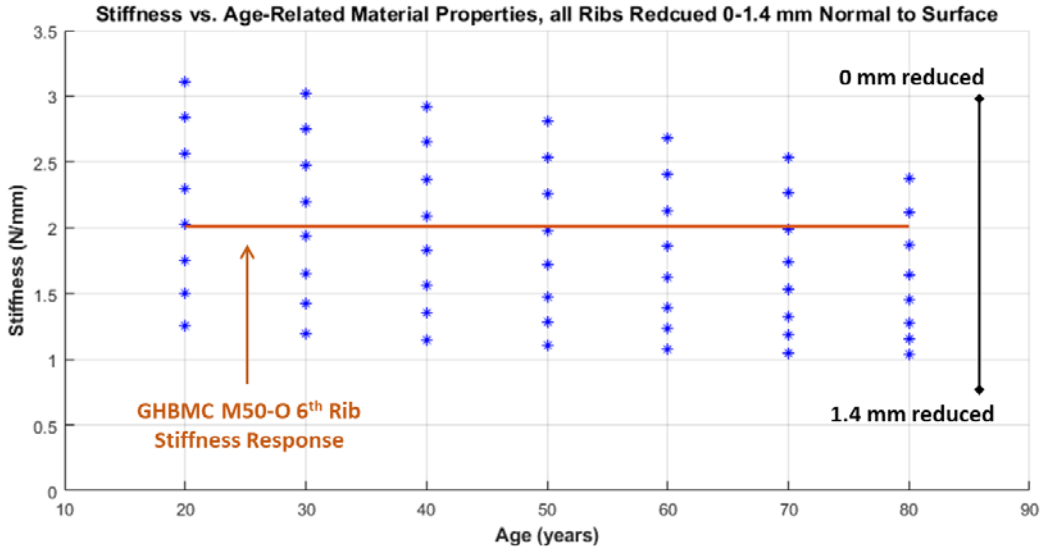

Fig. 6. Plotted data for stiffness vs. age-related material properties for all *nloc* 1 test runs. Highest data point in each age set represents no CSA reduction and lowest data point represents 1.4 mm projected inward, with each additional reduction step lying in between. The baseline GHBMC stiffness value in the v. 5.1.1 model, with *nloc* 1 by default and representing no specific age, is shown (2.01 N/mm).

IV. DISCUSSION

In studying the response of the 6th rib with varying rib size, age-dependent material properties, and shell element thickness projection direction, an array of mechanical responses was found. These range from low to high maximum forces experienced at the posterior rib end, fracture times, and stiffness values.

The most noticeable differences, which are backed up by statistical tests, were due to the differences in rib size obtained by varying Tt.Ar, followed closely by age-related material changes. Although the native model cortical thickness variation was not altered for a few reasons (to be discussed in the following paragraphs), overall enclosed area was reduced by adjusting *nloc*, which changed the response in bending. The data in [9] suggest the average overestimation along a normal of a rib element inwards would be approximately 0.8 mm. That study further suggests a 39% average overestimation in rib diameter but also notes that rib models may exhibit a more biofidelic response with an average of 0.8 mm reduction, which in the case of the GHBMC M50-O, is far less than a 39% reduction (0.8 mm accounts for a 24% reduction).

In terms of sample size for this study, we selected the step of 0.2 mm for a few reasons. First, it enabled us to sample uniformly and be sure that we had samples at the two key amounts of inward projection of 0.8 mm and 1.4 mm. Second, the value of 0.2 mm took into consideration the discretization of the structure. We wanted a step size that would adequately sample but was reasonable in light of element density, and this step is one order of magnitude below the average edge length of 2.3 mm. Remeshing was avoided, as we intend to maintain close to the existing element sizes for full HBMs. Lastly, the step had a statistical rationale. There was adequate significance in our multivariable regression with our existing samples, indicating an appropriate step size.

The GHBMC M50-O ribs were developed from a 26-YO male in terms of geometry, but the material properties utilised in the model represent no specific age. Comparing the data presented in Table AI of the appendix, it appears as though the baseline column (representing the response of the material properties of this baseline model) most closely matches the response of the age-related material properties for one of the older ages in almost all instances. This is likely due to the fact that most of the existing data on properties to which the material response was originally optimised when creating the GHBMC rib models was from a biased sample of PMHS at older ages. Now, given updated data that account for a more complete age range of PMHS, there are much more complete datasets that can be applied to future models.

Although we chose to study a number of dependent variables, stiffness was selected as the primary dependent variable of interest for discussion of this work because it provided a means of ranking rib models by structural response per the structural properties that were optimised in the initial generation of the GHBMC M50-O rib models. The work presented in [16] that precedes this study and generated the properties used in the models optimised elastic modulus, yield stress, tangent modulus, and failure strain of the ribs. Since elastic modulus was one of the variables optimised, which is analogous to stiffness when represented on a stress-strain curve, it was deemed an appropriate metric for comparison to altered test models. It would be inappropriate to represent overall mechanical response of the structure through one dependent variable, however. Stiffness is most likely the best choice when observing mechanical response in the elastic region of the bone's deformation, but when accounting for fracture, which occurs outside of this region, other variables such as energy absorbed and displacement at fracture are of note. For this reason, stiffness data was included in the body of the results; supplemental data can be found in the appendix. At a high level, in terms of energy, the baseline GHBMC model absorbs much less, and accordingly has a much lower displacement at fracture, than its age-related adjusted material properties counterparts.

As noted in Figure 6, we found the baseline rib with its current CSA, shell projection direction (proxy for second moment of area), and material properties is a reasonable representation of a broad swathe of our parametric study in terms of stiffness visually, when accounting for a range of possible geometries at each age. For instance, if the models were adjusted to a median age of approximately 40 years, with an inward projection of the mean value of 0.8 mm, the stiffness response would be quite similar to the baseline GHBMC M50-O model. Otherwise, the stiffness response of the baseline 6th rib model when extended to the extremes of the age range is still within the range of responses from the tested geometries. This aligns well with data from a recent study [19]. In this paper, it was reported that there was no strong correlation between age and stiffness response of the ribs, and that the best predictors of structural response were total enclosed area, cortical area, and bone distribution. This indicates that, when exploring aging effects and the necessity of their inclusion in constitutive rib models of HBMs, enclosed area, cortical area, and bone distribution changes with ages likely have an even greater effect than age-

related material properties. Enclosed area was found here to have a great effect in simulation response as well, and as such should be considered in future work in the context of age.

At least for this single rib example, the data also indicate that the peak force may be high and the displacement at failure low for the baseline GHBMC M50-O 6th rib. These observations are perhaps effects of the sample size of each study on which properties are based. Reference [16] optimised properties based on three ribs from each of three male PMHS (nine in total), whereas [15] used here included 61 specimens of both sexes and ranging in age 17-99. Other more recent studies in this area such as [19] have included much larger sample sizes. Although this provides insight into more robust experimental methods and may provide a basis for future updated models, the current GHBMC rib models are based on data presented in [16], so we must consider the direct underlying effects. There is a limitation in the current study as it was conducted at the single rib level, and accordingly, further study at the whole body level is needed.

This study was intended to determine which parameters would be statistically significant in modelling ribs when considering full-body HBMs at the full rib level. It should be noted that due to this wide range of responses observed in experimental studies, a biofidelic response at the whole body level might result from inputs that span a wide range themselves, at least in terms of structural response (including the baseline results). This is further confounded by the complex interplay within the HBM between materials, contacts, and hourglass control settings. Material and geometrical accuracy is paramount for failure criteria within components such as the ribs. As human modelling moves forward to focus on these more challenging and valuable aspects, highly accurate replication of the properties of these structures are likely going to be key.

Prior work has shown the importance of accurately reconstructing rib models for the purpose of precisely replicating response and fracture [6]. This study was not meant to replicate that work, rather to test the response of a rib as it exists in a typical whole body HBM. In this study, the number of elements was limited by the size of a typical element in the GHBMC M50-O rib model, which in turn is controlled by a desired minimum time step. These elements have a target edge length of approximately 3 mm (actually approximately 2.3 mm). The approach taken here exhibited a response representative of what we would expect to see in full HBMs and satisfied the objective of the study, which was to analyse the effect of these adjustments on the rib.

One clear limitation of this study is the omission of effects of the cortical thickness. The data used in the models were obtained from a dataset in reference [11] mentioned previously. New data have been presented in recent literature mapping rib cortical thickness using updated methods of CBM such as those by Holcombe et al. [8]. However, incorporation of these effects would have called for a new independent variable for thickness map, greatly increasing the modelling rigor of the study and the number of necessary test runs. Exploring these changes, therefore, was outside of the scope of this study, and looking into the effects of the CBM methods on the response of a single rib model would be one direction for future work. Instead, the area effect was analysed only via the *nloc* parameter, which could be seen as a proxy. The observation of the *nloc* variable as secondary or tertiary effect supports this assumption. Additionally, considering we are interested in material response resulting from rib models at targeted ages, a direction of future work will be to explore response on the basis of cortical thickness as it relates to effects of age. If we observe a decrease in cortical thickness with age, older aged models might experience more stress concentrations due to thinned cortex and higher fracture risk at lower forces given baseline material properties or the age-adjusted properties used as alterations in this study. Similar phenomena are explored experimentally in recent literature, and it would be of interest to see how the response translates to simulation as with other parameters [19]. Again, this introduces a greater number of variables and is outside the scope of this study, but it reiterates the demand for a future multivariate age-specific study in which enclosed area, material properties, and cortical thickness are all varied on the basis of age.

Nonetheless, one point worth noting about the trend in stiffness response with CSA reduction given the omission of cortical thickness changes is that shrinking the rib by reducing the enclosed area is creating a more slender rib in terms of robusticity. In other words, the ratio of bone diameter to bone length is decreasing. Since cortical thickness is not being changed, the ratio of Tt.Ar consisting of cortical bone is increasing, which is typical of more slender long bones. This phenomenon is discussed in detail in accordance with an experimental study presented in reference [5]. The cited research showed a positive correlation between robusticity and stiffness as well as between robusticity and peak force, which aligns with our findings of a negative correlation between CSA reduction and stiffness and CSA reduction and peak force. This is important to note because we did not account for the robusticity variable directly, as it came as a side effect of other geometry adjustments. However, we find

no discrepancy between the findings of this study and that of [5], which also notes that other studies conducted with a similar experimental dataset, such as [13] or [20], show that structural properties are not entirely explained by differences in age and sex. Given the goals of each of these studies, we sought to explore combined effects among ages in terms of age-related material properties along with geometry changes computationally to explore the effect on the response of HBMs.

Other avenues for future work besides those already mentioned have resulted from this study. The data collected in this study indicate that enclosed CSA and age-related material properties are factors that affect response; and this aligns with experimental data presented in recent literature [19]. We know that these parameters have an effect, and we are able to recreate this effect through simulation using computational models of the ribs. This provides a clear direction to take in updating these models based on the data reported in this study. HBMs such as the GHBMC models and similar models like THUMS are used throughout the community. It is critical, therefore, that new datasets [8][9][21] and functions [15][18] that are published in the literature be incorporated as updates into new releases of HBMs for continued increase of the biofidelity of these models.

Through PMHS validation testing at the denuded rib cage level, the current rib model in the GHBMC M50-O exhibits a reasonable stiffness response [22]. Consequently, the findings of this study indicate that the GHBMC M50-O rib model is a good starting point for a constitutive model at the individual rib level given its response relative to studied models that were updated per the recent literature (Figure 6). Nonetheless, the existing rib model would best be altered for models of targeted ages. The results suggest that adjusting parameters to match targeted ages will have a primary or secondary effect at the rib level (secondary to enclosed area), and in doing so, an inward projection may also be needed. One additional topic of future work, then, will be to assess how these changes affect the response at the whole body level and for injury prediction.

V. CONCLUSIONS

We found significant differences in the mechanical response of the 6th rib of an HBM due to CSA reduction, aging-based material property changes, and second moment of area adjustment. Reduced-Tt.Ar inward projection in steps of 0.2 mm was found to be a highly significant factor in six mechanical response values of the rib, and adjustments for age were found to be highly significant in five factors. Second moment of area was found to be significant but was generally a secondary or tertiary effect. The findings indicate that rib material and cross-sectional geometry considerations should be taken into account in the further development and refinement of age-specific HBMs. The existing GHBMC M50-O v 5.1.1 6th rib, with its initially generated Tt.Ar and material properties representing no specific age, behaves with a stiffness response similar to that of the rib of a younger male of roughly 20-40 years, given the age-related material property data and CSA reductions tested and no gross geometrical changes. The study has implications for human models whose ribs were generated through thresholding-based segmentation methods that have been demonstrated to overestimate rib CSA.

VI. ACKNOWLEDGEMENT

This work was funded by the Global Human Body Models Consortium, under contract WFU-006.

VII. REFERENCES

[1] Cavanaugh, J, "Accidental Injury: Biomechanics and Prevention", pages 362-390, Springer New York: New York, NY, 1993

[2] Novakov, I, Timonov, P, Stefanov, C, and Petkov, G. Rib fractures in blunt chest trauma-morbidity and mortality: self-experience study. *Trakia Journal of Science*, 2014. 12: p. 272-276

[3] Schoell, S, Weaver, A, et al. Functional outcomes of motor vehicle crash thoracic injuries in pediatric and adult occupants. *Traffic Injury Prevention*, 2018. 19(3): p. 280-286

[4] Kindig, M, Lau, A, and Kent, R. Biomechanical Response of Ribs Under Quasistatic Frontal Loading. *Traffic Injury Prevention*, 2011. 12(4): p. 377-387

[5] Murach, M, Kang, Y, et al. Rib Geometry Explains Variation in Dynamic Structural Response: Potential Implications for Frontal Impact Fracture Risk. *Annals of Biomedical Engineering*, 2017. 45(9): p. 2159-2173

[6] Iraeus, J, Lundin, L, et al. Detailed subject-specific FE rib modeling for fracture prediction. *Traffic Injury Prevention*, 2019. 20(sup2): p. S88-S95

[7] Charpail, E, Trosseille, X, et al. Characterization of PMHS ribs: a new test methodology. 2005, SAE Technical Paper.

[8] Holcombe, S, Kang, Y, Derstine, B, Wang, S, and Agnew, A. Regional maps of rib cortical bone thickness and cross-sectional geometry. *Journal of Anatomy*, 2019. 235(5): p. 883-891
[9] Holcombe, S, Kang, Y, Wang, S, and Agnew, A. The accuracy of local rib bone geometry measurement using fully body CT images. *Proceedings of IRCOBI Conference*, 2019. Florence
[10] Choi, H and Lee, I. Thorax FE model for older population. *Japanese Society of Mechanical Engineers*, 2009. 2009: p. 367-372
[11] Mohr, M, Abrams, E, Engel, C, Long, W, and Bottlang, M. Geometry of human ribs pertinent to orthopedic chest-wall reconstruction. *Journal of Biomechanics*, 2007. 40(6): p. 1310-1317
[12] Kemper, A, McNally, C, Pullins, C, Freeman, L, and Duma, S. The biomechanics of human ribs: material and structural properties from dynamic tension and bending tests. *Stapp Car Crash Journal*, 2007. 51: p. 235-273
[13] Agnew, A, Schafman, M, Moorhouse, K, White, S, and Kang, Y. The effect of age on the structural properties of human ribs. *Journal of the Mechanical Behavior of Biomedical Materials*, 2015. 41: p. 302-314
[14] Weaver, A, Schoell, S, and Stitzel, J. Morphometric analysis of variation in the ribs with age and sex. *Journal of Anatomy*, 2014. 225(2): p. 246-261
[15] Katzenberger, M, Albert, D, Agnew, A, and Kemper, A. Effects of sex, age, and two loading rates on the tensile material properties of human rib cortical bone. *Journal of the Mechanical Behavior of Biomedical Materials*, 2020. 102: p. 103410
[16] Li, Z, Kindig, M, et al. Rib fractures under anterior–posterior dynamic loads: experimental and finite-element study. *Journal of Biomechanics*, 2010. 43(2): p. 228-234
[17] Schoell, S, Weaver, A, Vavalle, N, and Stitzel, J. Age- and Sex-Specific Thorax Finite Element Model Development and Simulation. *Traffic Injury Prevention*, 2015. 16: p. S57-S65
[18] Li, Z, Kindig, M, Subit, D, and Kent, R. Influence of mesh density, cortical thickness and material properties on human rib fracture prediction. *Medical Engineering & Physics*, 2010. 32(9): p. 998-1008
[19] Agnew, A, Murach, M, et al. Sources of Variability in Structural Bending Response of Pediatric and Adult Human Ribs in Dynamic Frontal Impacts. *Stapp Car Crash Journal*, 2018. 62: p. 119-192
[20] Schafman, M, Kang, Y, et al. Age and sex alone are insufficient to predict human rib structural response to dynamic AP loading. *Journal of Biomechanics*, 2016. 49(14): p. 3516-3522
[21] Holcombe, S, Agnew, A, Derstine, B, and Wang, S. Comparing FE human body model rib geometry to population data. *Biomechanics and Modeling in Mechanobiology*, 2020
[22] Poulard, D, Kent, R, Kindig, M, Li, Z, and Subit, D. Thoracic response targets for a computational model: a hierarchical approach to assess the biofidelity of a 50th-percentile occupant male finite element model. *Journal of the Mechanical Behavior of Biomedical Materials*, 2015. 45: p. 45-64

VIII. APPENDIX

TABLE AI

RESULTS SORTED BY DIRECTION OF SHELL THICKNESS PROJECTION AND DEPENDENT VARIABLE. COLOUR GRADIENT SHOWS RANGE OF VALUES IN EACH SUB-TABLE FROM LOW (GREEN) TO HIGH (RED).

OUTPUT VARIABLE

Direction of Shell Thickness Projection

nloc 1

Displacement at Fracture (mm), nloc 1

CSA REDUCTION \ AGE	Baseline	20	30	40	50	60	70	80
Baseline	70.00	134.95	125.50	99.75	100.00	83.65	88.50	77.25
0.2 mm	70.65	152.85	128.45	117.05	114.35	84.00	92.20	75.35
0.4 mm	73.90	169.06	117.20	133.30	113.20	81.90	86.55	82.20
0.6 mm	93.45	141.25	124.95	111.45	112.45	86.90	100.40	88.20
0.8 mm	93.80	171.41	142.00	112.30	102.65	103.55	98.85	92.00
1.0 mm	105.10	165.71	173.96	168.81	133.30	113.00	115.65	105.85
1.2 mm	114.85	132.95	176.91	172.06	142.20	114.10	118.80	105.85
1.4 mm	112.75	180.76	176.50	173.81	161.61	111.95	116.50	105.25

Peak Force (N), nloc 1

CSA REDUCTION \ AGE	Baseline	20	30	40	50	60	70	80
Baseline	97.60	114.10	110.00	104.75	100.93	98.42	93.80	91.45
0.2 mm	88.43	105.90	101.71	98.24	94.27	91.80	87.79	84.53
0.4 mm	82.84	95.41	93.03	91.06	86.72	82.79	79.46	77.59
0.6 mm	76.88	89.73	86.74	83.92	80.71	77.31	74.98	71.81
0.8 mm	71.03	83.67	80.65	77.93	74.99	72.62	69.56	66.55
1.0 mm	65.79	76.47	74.26	71.03	68.51	65.93	63.65	61.17
1.2 mm	60.02	69.32	66.62	64.27	61.30	59.59	56.84	55.34
1.4 mm	53.29	62.44	61.30	57.75	55.55	53.73	51.60	49.32

Stiffness (N/mm), nloc 1

CSA REDUCTION \ AGE	Baseline	20	30	40	50	60	70	80
Baseline	2.01	3.11	3.02	2.92	2.81	2.69	2.54	2.38
0.2 mm	1.82	2.84	2.75	2.65	2.54	2.41	2.26	2.12
0.4 mm	1.63	2.56	2.47	2.37	2.25	2.12	1.99	1.87
0.6 mm	1.47	2.29	2.20	2.09	1.98	1.86	1.74	1.64
0.8 mm	1.34	2.03	1.93	1.83	1.72	1.62	1.53	1.45
1.0 mm	1.21	1.75	1.65	1.56	1.47	1.39	1.33	1.28
1.2 mm	1.10	1.50	1.42	1.35	1.28	1.23	1.19	1.16
1.4 mm	0.96	1.25	1.20	1.14	1.10	1.07	1.05	1.03

Displacement at Yield (mm), nloc 1

CSA REDUCTION \ AGE	Baseline	20	30	40	50	60	70	80
Baseline	41.90	31.90	31.26	31.66	31.12	31.64	31.80	33.10
0.2 mm	41.72	32.68	32.03	31.95	31.93	33.01	33.08	34.26
0.4 mm	43.81	32.92	32.61	33.77	33.83	33.76	34.52	36.12
0.6 mm	44.57	34.35	34.36	34.87	36.10	36.47	37.78	38.27
0.8 mm	45.68	35.78	36.21	37.24	38.03	39.32	39.73	39.55
1.0 mm	45.59	38.99	39.82	39.77	41.14	41.80	42.28	41.74
1.2 mm	46.00	40.60	40.97	41.81	42.04	42.52	42.16	41.27
1.4 mm	46.34	44.01	45.25	44.51	44.21	43.67	43.03	40.97

Force at Yield (N), nloc 1

CSA REDUCTION \ AGE	Baseline	20	30	40	50	60	70	80
Baseline	84.29	99.14	94.42	92.51	87.54	84.99	80.64	78.74
0.2 mm	75.92	92.68	88.02	84.67	80.94	79.40	74.90	72.58
0.4 mm	71.53	84.34	80.60	79.99	76.16	71.67	68.74	67.41
0.6 mm	65.69	78.75	75.53	72.95	71.31	67.70	65.79	62.73
0.8 mm	61.40	72.68	70.06	68.17	65.52	63.71	60.70	57.44
1.0 mm	55.17	68.14	65.90	62.09	60.51	58.17	56.04	53.27
1.2 mm	50.81	60.96	58.25	56.40	53.92	52.30	50.09	47.86
1.4 mm	44.63	55.12	54.16	50.86	48.76	46.85	45.10	42.32

Energy Absorbed (J), nloc 1

CSA REDUCTION \ AGE	Baseline	20	30	40	50	60	70	80
Baseline	4.48	12.44	11.16	8.33	8.02	6.24	6.42	5.15
0.2 mm	4.09	13.33	10.72	9.20	8.67	5.77	6.22	4.56
0.4 mm	3.97	13.73	8.85	10.05	7.94	5.06	5.21	4.67
0.6 mm	5.07	10.39	8.87	7.44	7.27	5.02	5.82	4.69
0.8 mm	4.62	11.90	9.44	6.91	5.93	5.75	5.19	4.50
1.0 mm	4.88	10.47	10.73	9.99	7.41	5.79	5.72	4.88
1.2 mm	4.94	7.45	9.91	9.29	7.17	5.27	5.29	4.37
1.4 mm	4.26	9.46	8.92	8.40	7.45	4.57	4.63	3.84

nloc 0

Displacement at Fracture (mm), nloc 0

CSA REDUCTION \ AGE	Baseline	20	30	40	50	60	70	80
Baseline	71.50	170.41	139.00	122.45	112.70	70.80	76.50	66.40
0.2 mm	75.15	176.11	167.21	126.70	113.85	74.25	80.25	69.05
0.4 mm	78.60	178.71	170.36	132.15	118.90	78.85	86.70	72.65
0.6 mm	85.45	181.71	177.46	137.10	120.85	86.55	96.55	76.60
0.8 mm	92.55	184.36	180.31	147.25	124.90	100.35	102.45	82.80
1.0 mm	102.45	186.06	182.81	179.06	131.30	102.55	104.35	88.55
1.2 mm	105.40	187.66	183.41	179.46	134.00	104.65	109.45	98.00
1.4 mm	108.25	188.56	184.50	180.71	140.45	107.10	110.00	100.90

Peak Force (N), nloc 0

CSA REDUCTION \ AGE	Baseline	20	30	40	50	60	70	80
Baseline	118.00	138.51	134.00	130.01	125.70	116.39	113.00	106.66
0.2 mm	109.56	127.73	124.32	119.74	115.76	107.84	104.94	99.02
0.4 mm	101.46	117.62	114.18	110.18	106.73	100.01	97.52	91.76
0.6 mm	94.40	108.01	104.61	101.01	97.53	92.70	90.46	84.92
0.8 mm	87.14	98.78	95.57	92.15	89.06	85.65	82.88	78.31
1.0 mm	79.93	89.81	86.86	84.19	81.07	77.98	75.36	71.88
1.2 mm	72.43	81.10	78.31	75.67	73.26	70.56	68.21	65.81
1.4 mm	65.43	73.65	71.10	68.55	66.45	64.10	62.00	59.41

Stiffness (N/mm), nloc 0

CSA REDUCTION \ AGE	Baseline	20	30	40	50	60	70	80
Baseline	2.70	3.95	3.78	3.61	3.44	3.27	3.11	2.97
0.2 mm	2.45	3.56	3.40	3.23	3.06	2.92	2.79	2.68
0.4 mm	2.23	3.20	3.07	2.93	2.79	2.68	2.57	2.47
0.6 mm	1.97	2.81	2.69	2.57	2.46	2.37	2.28	2.19
0.8 mm	1.77	2.49	2.38	2.29	2.20	2.12	2.06	1.98
1.0 mm	1.51	2.22	2.14	2.07	2.00	1.92	1.85	1.77
1.2 mm	1.34	1.93	1.86	1.79	1.74	1.68	1.63	1.56
1.4 mm	1.12	1.73	1.67	1.62	1.56	1.50	1.44	1.35

Displacement at Yield (mm), nloc 0

CSA REDUCTION \ AGE	Baseline	20	30	40	50	60	70	80
Baseline	37.09	31.29	31.59	31.76	32.16	30.77	31.54	30.78
0.2 mm	37.68	32.08	32.61	32.84	33.26	32.04	32.57	31.75
0.4 mm	38.41	32.80	33.22	33.41	33.71	32.50	32.73	31.65
0.6 mm	40.56	34.32	34.73	34.92	35.07	34.27	34.47	33.08
0.8 mm	42.01	35.46	35.90	35.87	35.86	35.34	35.09	33.87
1.0 mm	45.94	36.21	36.28	36.32	36.00	35.62	35.42	35.07
1.2 mm	46.64	37.39	37.41	37.73	37.52	36.94	36.78	36.35
1.4 mm	50.66	37.70	37.63	37.79	37.77	37.55	37.79	38.41

Force at Yield (N), nloc 0

CSA REDUCTION \ AGE	Baseline	20	30	40	50	60	70	80
Baseline	99.96	123.57	119.55	114.80	110.47	100.62	98.06	91.39
0.2 mm	92.36	114.08	110.75	106.07	101.93	93.71	90.98	85.05
0.4 mm	85.76	105.10	101.88	97.79	94.07	87.01	84.26	78.13
0.6 mm	79.73	96.62	93.50	89.90	86.41	81.12	78.73	72.57
0.8 mm	74.17	88.45	85.46	82.19	78.96	75.05	72.26	67.20
1.0 mm	69.17	80.45	77.76	75.25	72.05	68.54	65.70	61.94
1.2 mm	62.59	72.10	69.46	67.71	65.20	62.14	59.91	56.68
1.4 mm	56.98	65.22	62.76	61.28	59.11	56.36	54.34	51.68

Energy Absorbed (J), nloc 0

CSA REDUCTION \ AGE	Baseline	20	30	40	50	60	70	80
Baseline	5.72	20.69	15.90	13.17	11.47	6.05	6.49	5.07
0.2 mm	5.59	19.79	18.06	12.62	10.69	5.93	6.30	4.91
0.4 mm	5.45	18.50	16.95	12.19	10.35	5.89	6.40	4.83
0.6 mm	5.59	17.27	16.27	11.66	9.66	6.09	6.73	4.73
0.8 mm	5.68	16.02	15.11	11.56	9.17	6.71	6.61	4.79
1.0 mm	5.91	14.71	13.94	13.15	8.84	6.26	6.14	4.74
1.2 mm	5.52	13.42	12.64	11.91	8.18	5.80	5.88	4.88
1.4 mm	5.13	12.21	11.54	10.85	7.80	5.37	5.35	4.55

TABLE AII

SUPPLEMENTARY RESULTS FOR ALL *NLOC* 1 TEST RUNS AS DISPLAYED IN LEFT COLUMN OF TABLE AI. PLOTS OF EACH DEPENDENT VARIABLE AGAINST CSA REDUCTION ARE DISPLAYED IN THE LEFT COLUMN, AND PLOTS OF EACH DEPENDENT VARIABLE AGAINST AGE (BY MATERIAL PROPERTIES) ARE DISPLAYED IN THE RIGHT COLUMN. VERTICAL POINTS REPRESENT CHANGES IN EITHER AGE (AT LEFT) OR CSA REDUCTION (AT RIGHT). DISPLACEMENT ABBREVIATED AS DISP.

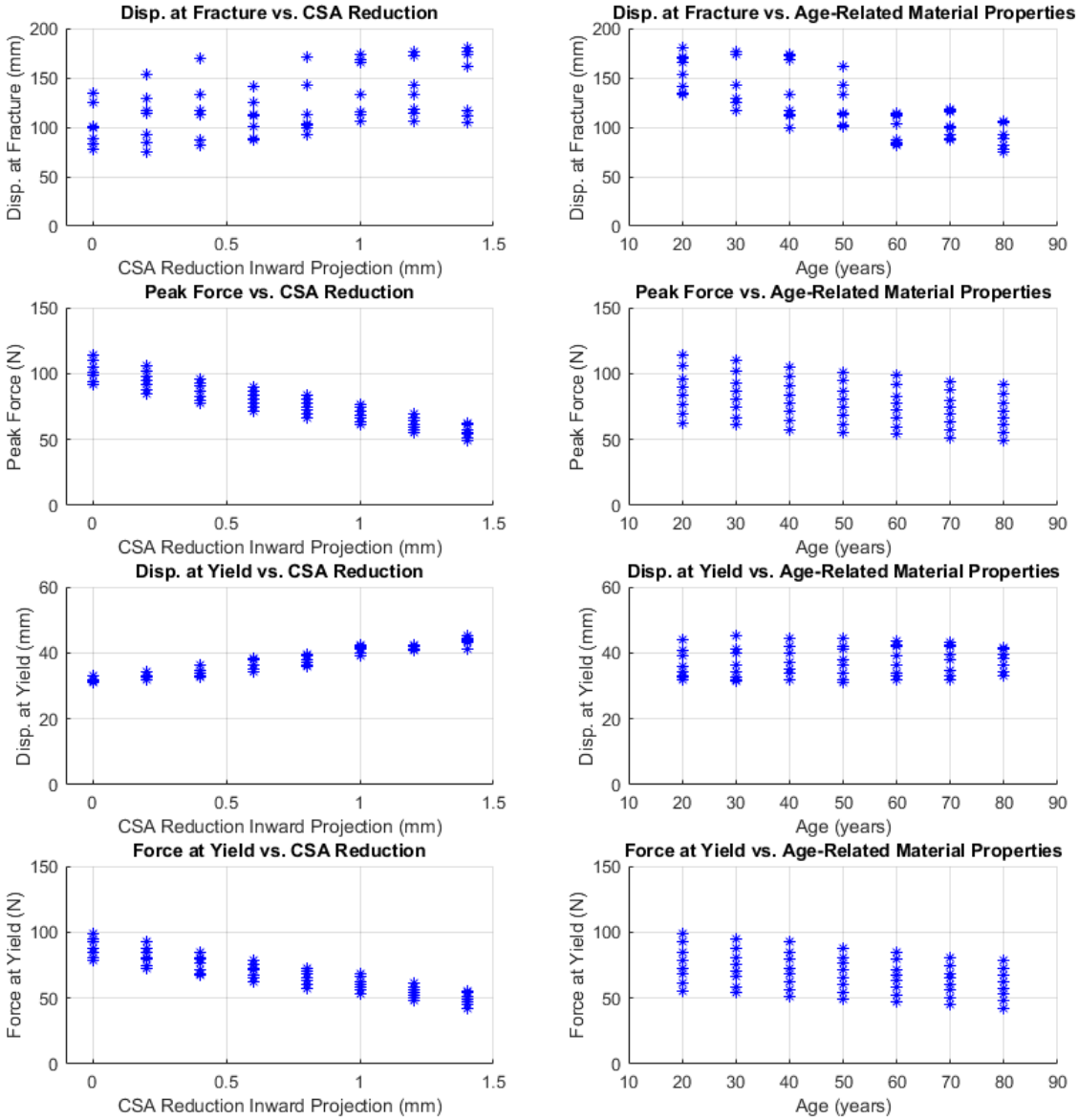

TABLE AIII

SUPPLEMENTARY RESULTS FOR ALL *NLOC* 0 TEST RUNS AS DISPLAYED IN LEFT COLUMN OF TABLE AI. PLOTS OF EACH DEPENDENT VARIABLE AGAINST CSA REDUCTION ARE DISPLAYED IN THE LEFT COLUMN, AND PLOTS OF EACH DEPENDENT VARIABLE AGAINST AGE (BY MATERIAL PROPERTIES) ARE DISPLAYED IN THE RIGHT COLUMN. VERTICAL POINTS REPRESENT CHANGES IN EITHER AGE (AT LEFT) OR CSA REDUCTION (AT RIGHT). DISPLACEMENT ABBREVIATED AS DISP.